PERGAMON

International Journal of Solids and Structures 38 (2001) 3905–3925

INTERNATIONAL JOURNAL OF SOLIDS and STRUCTURES

www.elsevier.com/locate/ijsolstr

Micro-mechanics of off-axis loading of metal matrix composites using finite element analysis

M.M. Aghdam [a], M.J. Pavier [b,*], D.J. Smith [b]

[a] *Department of Mechanical Engineering, Amir Kabir University of Technology, Hafez Avenue, Tehran, Iran*
[b] *Department of Mechanical Engineering, University of Bristol, Queen's Building, University Walk, Bristol BS8 1TR, UK*

Received 24 January 2000

Abstract

A three-dimensional, finite element, micro-mechanical model has been developed to predict the behaviour of unidirectional metal matrix composites subjected to off-axis loading. The model consists of a unit cell, representing a quarter fibre surrounded by matrix as a repeating element in a square array of fibres. Boundary conditions have been developed to allow the simultaneous application of axial shear, normal and transverse loading and thermal residual stress. The model includes the important effects of de-bonding of the interface between fibre and matrix, friction between fibre and matrix and the presence of thermal residual stress. The results of the model have been compared with experimental stress–strain data for a SiC/Ti composite system loaded at various off-axis angles between 0° and 90°. There is good agreement between the model and experiment for Young's modulus, elastic limit and ultimate strength. It is demonstrated that for a model to predict correctly the composite strength when the fibre is perfectly de-bonded from the matrix, friction must be introduced at the interface.

Keywords: Micro-mechanics; Metal matrix composites; Off-axis loading; Finite element analysis

1. Introduction

Off-axis loading takes place when a unidirectional composite is loaded in a direction other than the fibre direction. As the loading direction is varied from directly in line with the fibre axis to normal to the fibre axis, the behaviour of the composite changes from fibre dominated to matrix dominated. Off-axis testing is therefore a straightforward technique that can be used to characterise a wide range of properties of a composite material. The off-axis test is particularly useful since it assesses the ability of the composite to preserve its properties when it is not loaded in the optimum fibre direction. Understanding the manner in which the properties degrade as the loading conditions vary is an essential requirement in the practical use of composites.

In off-axis loading, a uniaxial load is applied to a coupon where the fibres are aligned at an angle θ to the loading direction as shown in Fig. 1(a). Two co-ordinate systems are defined: the (1, 2) system, where the 1

* Corresponding author. Tel.: +44-0117-928-8211; fax: +44-0117-929-4423.
E-mail address: martyn.pavier@bristol.ac.uk (M.J. Pavier).

0020-7683/01/$ - see front matter
PII: S0020-7683(00)00248-1

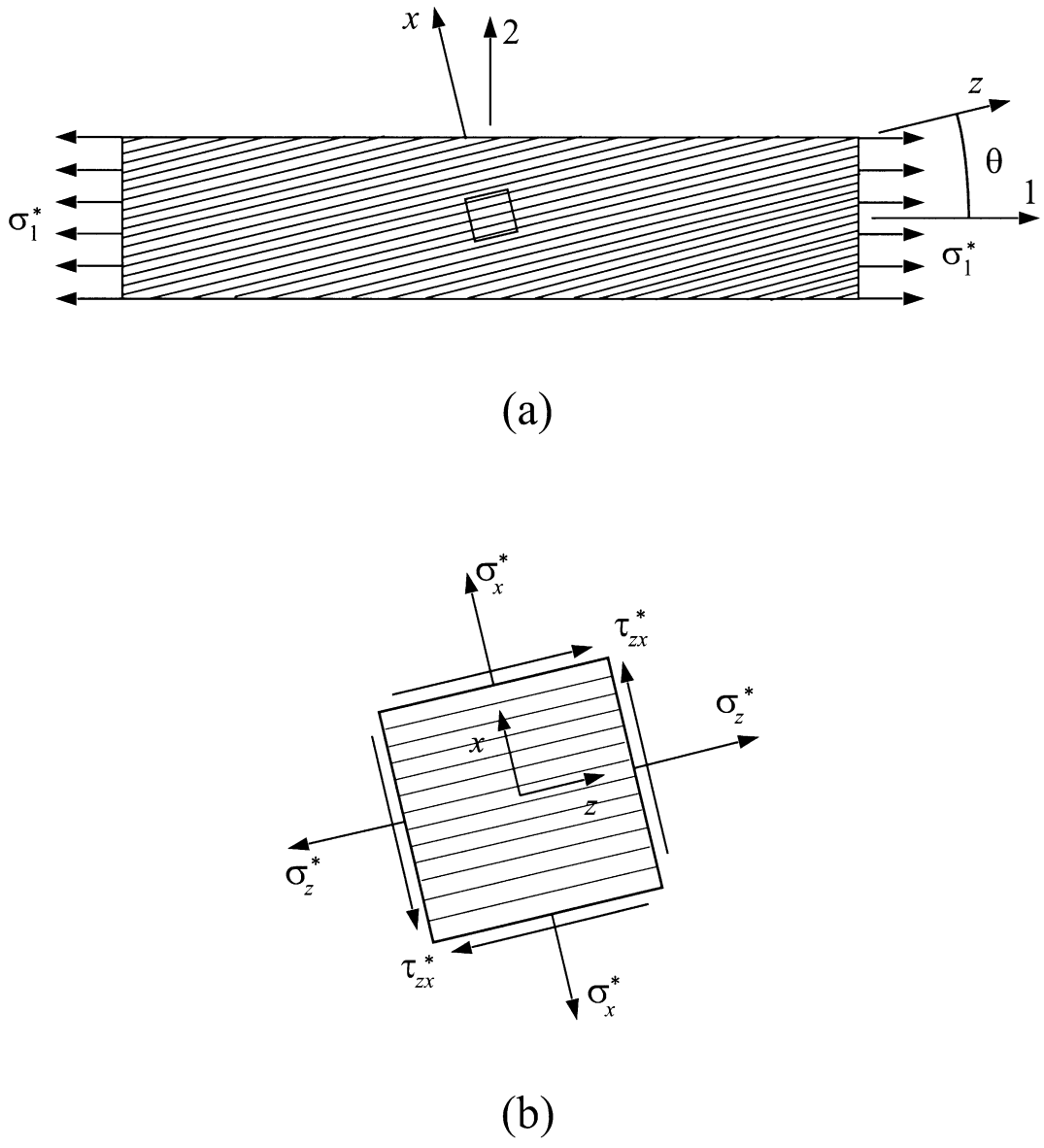

Fig. 1. Typical off-axis tensile test configuration: (a) specimen geometry and loading and (b) stresses in material co-ordinate.

direction is the loading direction, and the (x, y, z) system, where the z axis coincides with the fibre direction and the x–y plane is perpendicular to the fibres.

The stress state within the specimen in the material principal axes consists of three stress components: axial σ_z^*, transverse σ_x^*, and axial shear τ_{zx}^* as indicated in Fig. 1(b). The superscribed asterix signifies that these stresses are average stresses applied to a sufficiently large volume of the composite. These stress components can be determined from the stress applied to the composite using the following transformation equations:

$$\sigma_x^* = \frac{\sigma_1^*}{2}(1 - \cos 2\theta),$$
$$\sigma_z^* = \frac{\sigma_1^*}{2}(1 + \cos 2\theta), \tag{1}$$
$$\tau_{zx}^* = -\frac{\sigma_1^*}{2}\sin 2\theta,$$

where σ_x^*, σ_z^*, and τ_{zx}^* are the average normal and shear stresses in the material co-ordinate system and σ_1^* is the average applied stress, that is, the load applied to the specimen divided by the cross-sectional area. Using the transformation equations, the average material direction stresses can be evaluated knowing the off-axis angle and the applied load. Critical material stress components may then be inferred from the failure load of the specimen.

Off-axis loading has been studied theoretically at both the micro-mechanical and continuum level. At the micro-mechanical level, the composite is treated as a heterogeneous material consisting of fibres embedded in a matrix material. At a continuum level, however, the composite is presumed to be a material which is macroscopically homogeneous and generally orthotropic. Composite structures such as plates and shells, normally composed of various plies oriented in specific directions to obtain a particular behaviour, are studied at the continuum level.

A number of continuum models have been proposed to predict the behaviour of composite materials subjected to off-axis loading. Among the earlier efforts to study such behaviour are the analytical and experimental studies carried out by Stowell and Liu (1961), Kelly and Davis (1965), Jackson and Cratchley (1966), Cooper (1966), and Pipes and Cole (1973).

Determination of the shear properties of the composite has been of particular interest in off-axis loading. The off-axis tension test at 10° to the fibre direction was first proposed by Chamis and Sinclair (1976,1977) for shear characterisation of unidirectional fibre reinforced composites. They performed both theoretical and experimental studies to assess the applicability of the test for obtaining axial shear parameters. Pindera and co-workers (1986,1987,1989) recommended a 45° off-axis tensile test to measure the shear modulus and a 0° Iosipescu specimen to measure the shear strength. Their model was mainly developed to relate the apparent axial shear stress to the actual shear stress in an off-axis test specimen. The difference between apparent axial shear and actual shear properties arises due to end constraint effects during off-axis loading. In off-axis loading, there is a rotational tendency in the specimen as a result of shear coupling effects. Therefore, clamped supports of the specimen create additional shear stresses within the specimen. The effect of the end constraint has also been discussed by Pagano and Halpin (1968) and Rizzo (1969).

Many attempts have been made to develop micro-mechanical models for predicting the behaviour of composites subjected to various types of loading. The effect of thermal residual stresses arising from manufacture of the composite and imperfect bonding of the interface between fibre and matrix have been included. Most of these studies are limited to the application of normal loading in the transverse and axial directions (Nimmer, 1990; Wisnom, 1990; Zahl et al., 1994; Du and Zok, 1998; Aghdam et al., 2000). In addition, some studies have considered shear loading (Adams and Doner, 1967; Naik and Crews, 1993; Sun and Vaidya, 1996). However, inclusion of thermal residual stresses is much more difficult in a shear analysis since the boundary conditions for shear loading are asymmetric, while those for the prediction of thermal residual stress are symmetric. Nedele and Wisnom (1994) developed an approximate solution for this problem. Later Aghdam et al. (1998) presented an exact method to apply combinations of thermal, shear, axial and transverse loadings.

Micro-mechanical modelling of off-axis loading in particular has received relatively little attention. Aboudi (1988) used his analytical micro-mechanical model to predict the strength of a unidirectional composite under complex loading. The failure of the interface was also considered in his study. The off-axis strength of various polymeric and metallic composite systems were predicted and compared with the

available experimental data. Similar results together with some transverse and off-axis creep test of various composite systems were also presented by Aboudi (1989).

In a study by Foye (1973), a finite element, micro-mechanical model was developed for composite laminates subjected to a general combination of normal and shear stresses. A rectangular fibre packing geometry and perfect bonding between the fibre and matrix were considered in the model. Thermal residual stresses arising from manufacture were not included in the analysis. The effects of non-linear coupling that can exist between shear and normal stresses when the composite is loaded in combined shear and normal loads were investigated. No comparison with any other experimental or analytical investigation was given in the paper. Although the off-axis test was not considered in the paper, it appears that the general approach could be used for off-axis loading. However, details of the boundary conditions used for combinations of shear and normal loading were not provided.

Another finite element study for combined loading conditions including axial shear was presented by Adams and Crane (1984a,b). Their model used a generalised plane strain finite element analysis, a modified version of the classical generalised plane strain formulation introduced by Lekhnitskii (1963). A perfectly bonded interface and rectangular array of fibres were assumed. Methods were used to include axial shear without altering the generalised plane strain condition. Comparisons with experimental data were provided for $\pm 45^\circ$ laminates. Although the modified two-dimensional (2-D) model was sufficient to analyse specific combined loading cases, a full three-dimensional (3-D) analysis was recommended by the authors for general purposes (Adams and Crane, 1984a).

This paper presents the results of a finite element, micro-mechanical model of metal matrix composites (MMCs) subjected to off-axis loading. First, a 2-D model is described for the more simple case of axial and transverse loading. Next, a full 3-D, finite element, micro-mechanical model is presented for general combinations of axial shear, axial and transverse normal load. This model is used to analyse unidirectional composites under off-axis loading, a special case of these general loading conditions. Boundary conditions are developed, allowing both thermal and mechanical loading to be applied simultaneously. Various interface conditions between fibre and matrix are considered from perfectly bonded to de-bonded with frictional contact conditions.

The micro-mechanical model is used to predict the behaviour of a SiC/Ti MMC subjected to off-axis loading. Results obtained for the stress–strain response, off-axis Young's modulus, onset of non-linear behaviour and strength are compared with other continuum models and experimental data from Thomas (1997).

2. Axial and transverse loading

In this section, 2-D, finite element, micro-mechanical models will be described for predicting the behaviour of the composite in axial and transverse loading. These cases correspond to the two limits for off-axis loading, when the off-axis angle θ is either 0° or 90°. The general case for off-axis loading requires a 3-D model, which will be described in a subsequent section. Predictions for the stress–strain curves of the material in tension and compression will be compared with the existing experimental results. The results presented in this section for axial and transverse loading are special cases of general biaxial loading of MMCs (Aghdam et al., 2000).

2.1. Material properties

The composite system chosen for the numerical investigation consists of a titanium alloy matrix, IMI 318 (Ti–6Al–4V), reinforced by aligned DERA Sigma SM1240, SiC fibres. Fibres were assumed to be temperature independent and elastic up to the fracture point. The fracture strength has been reported to be

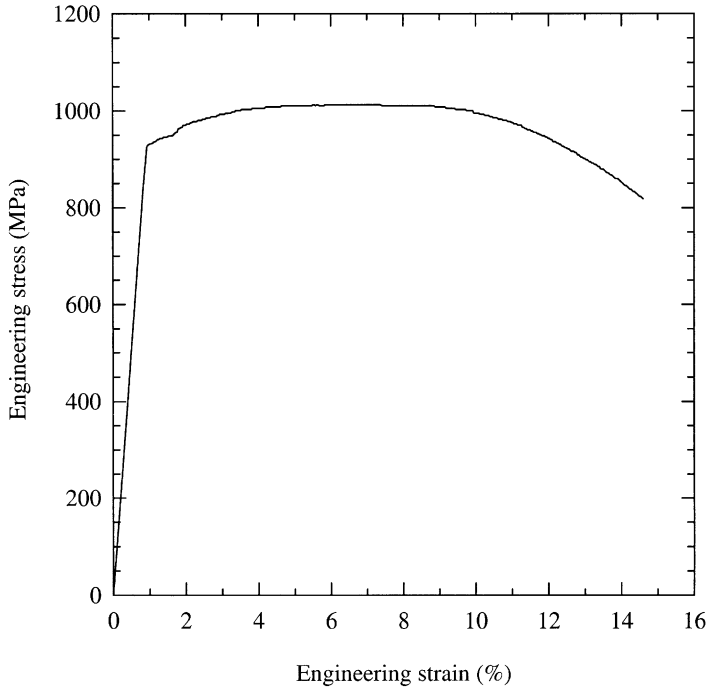

Fig. 2. Room temperature stress–strain response of titanium IMI 318.

between 3 and 4 GPa in tension (Le Petitcorps et al., 1988) and 8–10 GPa in compression (Spowart and Clyne, 1999). A value of 409 GPa was used for Young's modulus of the fibres, 0.2 for Poisson's ratio and 5.0×10^{-6} K^{-1} for the coefficient of thermal expansion.

The matrix, IMI 318, was assumed to have temperature dependent elastic properties. The room temperature Young's modulus of the matrix was taken to be 107 GPa and Poisson's ratio as 0.3. The room temperature stress–strain curve of the matrix is shown in Fig. 2, (IMI Titanium Limited brochure, 1993). The dependency of the coefficient of thermal expansion and Young's modulus with temperature is given in Tables 1 and 2.

The fabrication process of the composite by diffusion bonding takes place in the range 850–930°C (Calvo et al., 1992). In the analyses where a residual stress arising from the fabrication process is included, the fibre and matrix were assumed to be stress free at 930°C. This state of residual stress will be an upper bound since any relaxation of the residual stresses due to creep or plasticity is ignored. However, it is not believed that the calculated state of residual stress is unrealistically high, since values are of the order of those measured by X-ray (Jansson et al., 1991).

Table 1
Mean coefficient of thermal expansion (CTE) of IMI 318

Temperature (°C)	Mean CTE (10^{-6} K^{-1})
20–200	9.0
20–300	9.5
20–400	9.8
20–500	10.0
20–900	10.4

Table 2
Temperature dependent Young's modulus of IMI 318

Temperature (°C)	Young's modulus (GPa)
23	107.0
100	102.0
200	96.0
300	90.0
400	85.0
500	79.0

2.2. Representative volume element

In a real unidirectional fibre reinforced composite the fibres are arranged randomly. Since it is difficult to model this random arrangement, the composite is idealised as a periodic array of fibres, usually, in a square or a hexagonal array. The smallest repeating area of the cross-section is selected as the representative volume element (RVE) and it is assumed that the global behaviour of the composite is the same as that of the RVE. Here a square array of fibres in matrix was assumed, with a quarter of the fibre and the corresponding matrix as shown in Fig. 3 chosen for the RVE. Generalised plane strain elements of six-noded triangular and eight-noded quadrilateral geometries were used in the mesh.

2.3. Boundary conditions

For the prediction of thermal residual stress, the deformation of the RVE is compatible with a generalised plane strain condition where strain in the fibre direction is constant. Therefore, 2-D generalised plane strain elements in ABAQUS (1997) were used to mesh the geometry of the RVE shown in Fig. 3. The required boundary conditions for thermal residual stress have been described by several researchers (Nimmer, 1990; Wisnom, 1990; Chandra et al., 1994). These boundary conditions included symmetric constraints on nodes on the left and bottom sides of the RVE to represent the rest of the body. In addition, all nodes on the other sides were constrained to have equal displacements perpendicular to the side on which they lie.

For axial or transverse loading, a generalised plane strain analysis was again suitable, with the same boundary conditions as for thermal residual stress. Therefore, it was simple to combine the analysis of thermal residual stress with the behaviour of the composite subjected to axial or transverse loading. The boundary conditions for axial or transverse loading can be expressed as

$$\begin{aligned} u_x(0,y) &= 0, \\ u_x(a,y) &= a\overline{\varepsilon}_x, \\ u_y(x,0) &= 0, \\ u_y(x,a) &= a\overline{\varepsilon}_y, \end{aligned} \tag{2}$$

where for example, $u_x(0,y) = 0$ is the x displacement of nodes on the left hand side of the RVE, $\overline{\varepsilon}_x$ is the applied normal strain in the x direction and a is the width of the RVE. For a generalised plane strain element, constraining an additional degree of freedom representing the strain normal to the plane of the element simulated the application of load in the axial direction.

2.4. Interface conditions

The transverse strength of MMCs is often limited by the weak interface between fibres and matrix (Johnson et al., 1990; Newaz and Zhang, 1998). The effect of the weak interface was studied by interposing

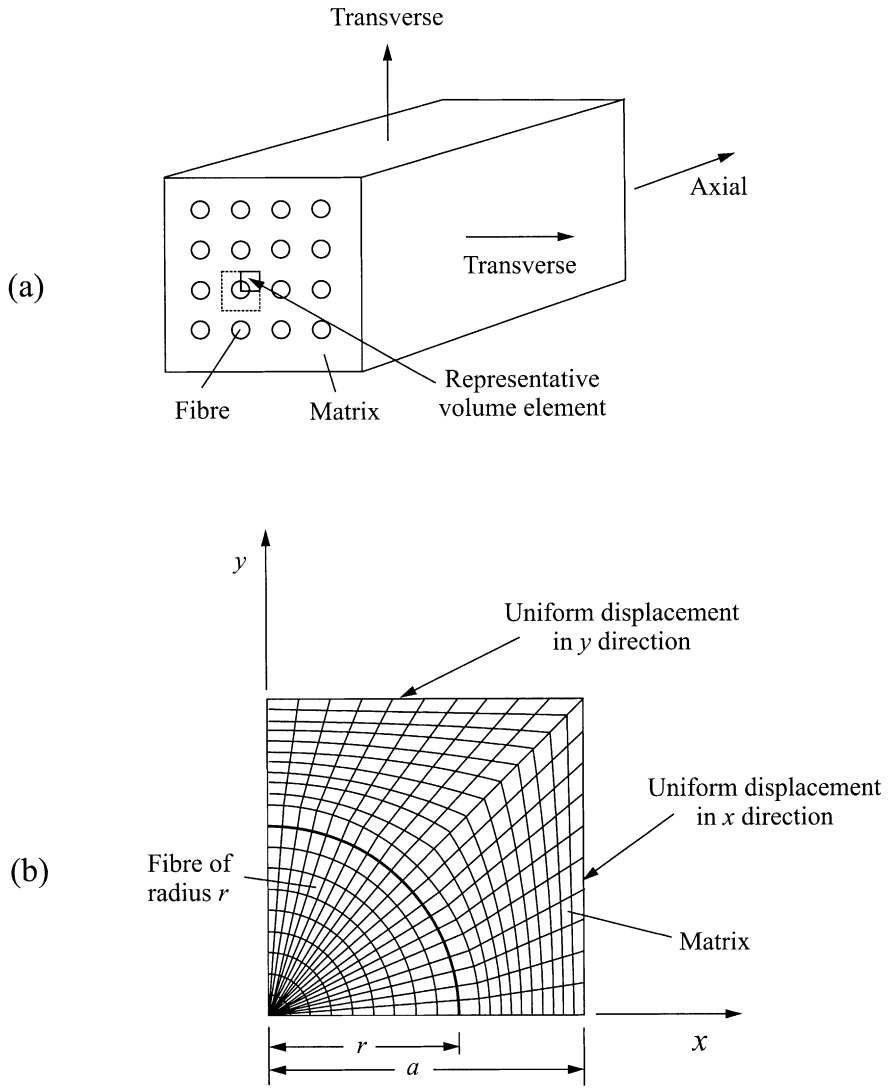

Fig. 3. Finite element model for on-axis loading: (a) RVE for a square array of fibres and (b) the finite element mesh for the RVE.

two sets of special contact elements along the boundary between the fibre and matrix with two extreme conditions being considered: a perfectly bonded interface and a completely de-bonded interface. For the perfectly bonded condition, the contact surfaces were simply tied to each other which constrained all nodes on one surface to have the same displacements as the other surface. For a completely de-bonded interface, only compressive stresses can be transferred between the fibre and matrix.

2.5. Results and discussion

Using the finite element, micro-mechanical model, stress–strain curves were predicted for MMCs loaded in the axial and transverse direction. Curves were produced for tensile and compressive loading, with and

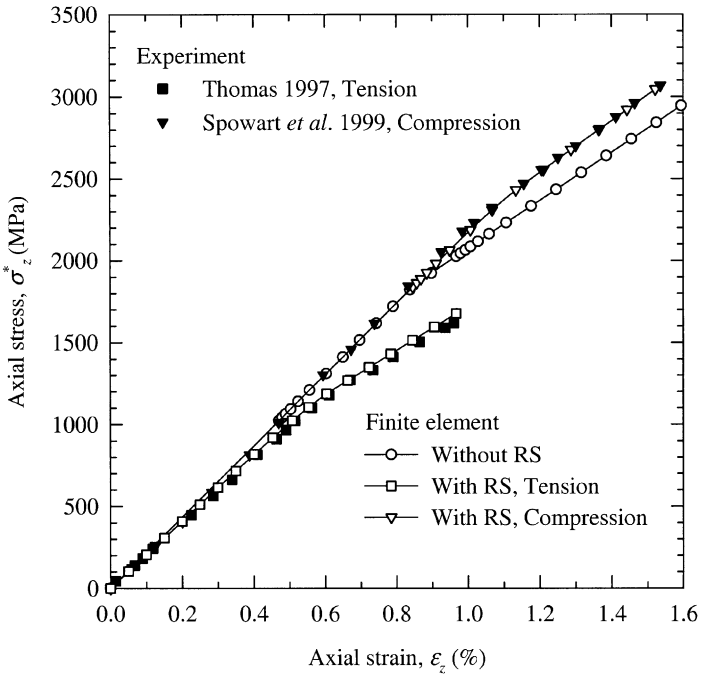

Fig. 4. Predicted and experimental stress–strain curves for longitudinal loading in tension and compression.

without thermal residual stress and with different interface conditions. Uniform thermal residual stresses of 798 MPa in compression and 430 MPa in tension were predicted in the fibre and matrix in the axial direction.

When loaded in the axial direction, the model predicted that the stress–strain curves are influenced by thermal residual stresses but not significantly by the different interface conditions. Fig. 4 shows the stress–strain response for the micro-mechanical model of the composite without thermal residual stress and with residual stress in tension and compression. As observed in the experimental work reported by Clyne and Withers (1993), the model exhibited a difference in behaviour when loaded in tension and compression if the thermal residual stresses were included. Fig. 4 also shows experimental measurements for MMCs loaded in tension (Thomas, 1997) and loaded in compression (Spowart and Clyne, 1999). Excellent agreement can be observed with the predictions of the model. The small change in Young's modulus between the tensile and compressive results is due to the slight difference in volume fraction used in the two sets of experimental tests: 0.33 for the tensile tests and 0.35 for the compressive tests.

The presence of residual stresses and the interface condition both affect the predicted behaviour of the composite in transverse loading. Fig. 5 shows the stress–strain curve for the model with a bonded interface without residual stress and with residual stress in tension and compression. Again, a difference in behaviour in tension and compression only occurred when residual stresses were included. All three curves reach a plateau when the matrix becomes fully plastic: this plateau does not depend on whether residual stress is included. The limiting transverse stress σ_z^* for the material is approximately given by

$$\sigma_z^* = \frac{2\sigma_0}{\sqrt{3}}, \tag{3}$$

where σ_0 is the uniaxial yield stress of the matrix (Zahl et al., 1994). Taking a value for σ_0 of 930 MPa gives a limiting transverse stress σ_z^* of 1074 MPa.

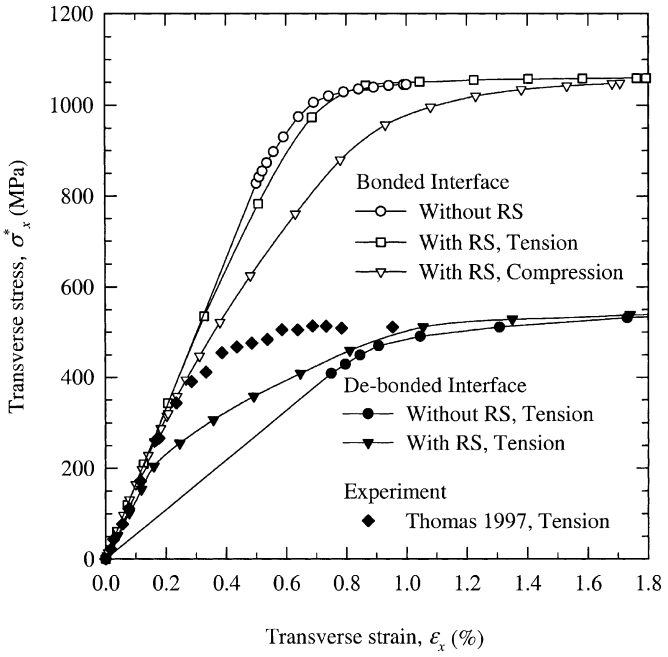

Fig. 5. Predicted and experimental stress–strain curves for transverse loading in tension and compression.

For the case of a de-bonded interface, only results for tensile loading are shown. Residual stress retarded the separation of the matrix from the fibre until the transverse stress reached about 200 MPa. Thereafter, the slope of the curve reduced until it met the curve without residual stress. Both curves reach a plateau, but at a stress of about a half of that for the bonded interface. Again, an approximation exists for the limiting transverse stress:

$$\sigma_z^* = \frac{2\sigma_0}{\sqrt{3}}\left[1 - \sqrt{2\sqrt{3}\frac{f}{\pi}}\right], \tag{4}$$

where f is the fibre volume fraction (Du and Zok, 1998). For a fibre volume fraction of 0.33, the limiting transverse stress is calculated to be 700 MPa.

Also, included in the figure are the experimental results provided by Thomas (1997). At low stresses, the experimental curve follows the model curve for the bonded interface but eventually separation of the interface occurred and the experimental curve joins the model for the de-bonded interface. In the experiments, separation of the interface occurred at a higher stress than would be predicted for a de-bonded interface with residual stress. The interface in the real material certainly has some strength, therefore, but no attempt has been made here to model their strength. Rather, the property of the interface has been bounded between the two extremes of a perfect bonding and perfect de-bonding.

3. Off-axis loading

A 3-D, finite element, micro-mechanical model will now be described for predicting the behaviour of the composite in general off-axis loading. Predictions for the stress–strain curves of the material in tension for a number of intermediate off-axis angles will be compared with experimental results. The variation of elastic

modulus, elastic limit and tensile strength with off-axis angle will then be compared with experimental results.

3.1. Representative volume element

Off-axis loading of the RVE includes axial and transverse normal stress and axial shear stress. Due to the axial shear loading, the deformation of the RVE in the fibre direction varies and a 2-D model becomes difficult to use. Therefore, a 3-D model consisting of a single layer of elements in the axial direction was used with the same arrangement of elements in the transverse plane as in Fig. 3. A combination of 15-noded triangular prism elements and 20-noded brick elements was used to construct the geometry of the mesh. Although, in this study only the square array was considered, the method is general and can also be used for square-diagonal and hexagonal fibre packing.

3.2. Boundary conditions

For off-axis loading, three different stress components must be applied simultaneously to the RVE as shown in Fig. 6. The relative magnitude of these stress components is calculated using Eq. (1) and depends on the off-axis angle θ. While the axial shear term requires a boundary condition where displacements vary in the fibre direction, the axial stress term requires a boundary condition that displacements are uniform. The essential task in developing a micro-mechanical model for off-axis loading is to find a method for applying these apparently incompatible boundary conditions simultaneously.

To specify the constraints for the model, the origin of a co-ordinate system was chosen as the midpoint of the RVE as shown in Fig. 7(a). Tensile axial load results in a relative displacement of the surfaces (x, y, l) and $(x, y, -l)$ apart from each other. For axial shear loading, the surface (a, y, z) has a displacement with respect to the surface $(0, y, z)$ in the axial direction. The effect of axial shear load is such that all nodes with the same position in the x–y plane have the same displacement in the z direction. These boundary conditions can be expressed as

$$\begin{cases} u_z(x,y,l) = -u_z(x,y,-l) = l\bar{\varepsilon}_z & \text{due to axial load,} \\ \begin{cases} u_z(x,y,l) = u_z(x,y,-l) \\ u_z(a,y,z) - u_z(0,y,z) = a\bar{\gamma}_{zx} \end{cases} & \text{due to axial shear,} \end{cases} \tag{5}$$

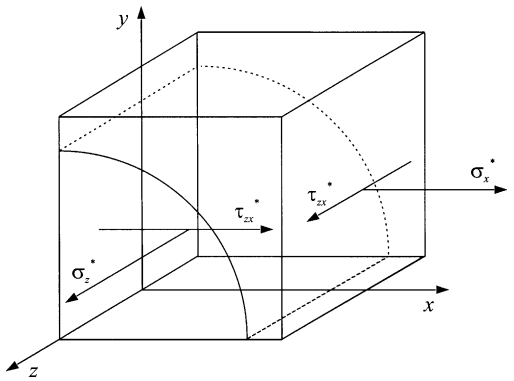

Fig. 6. RVE for off-axis loading and related stresses.

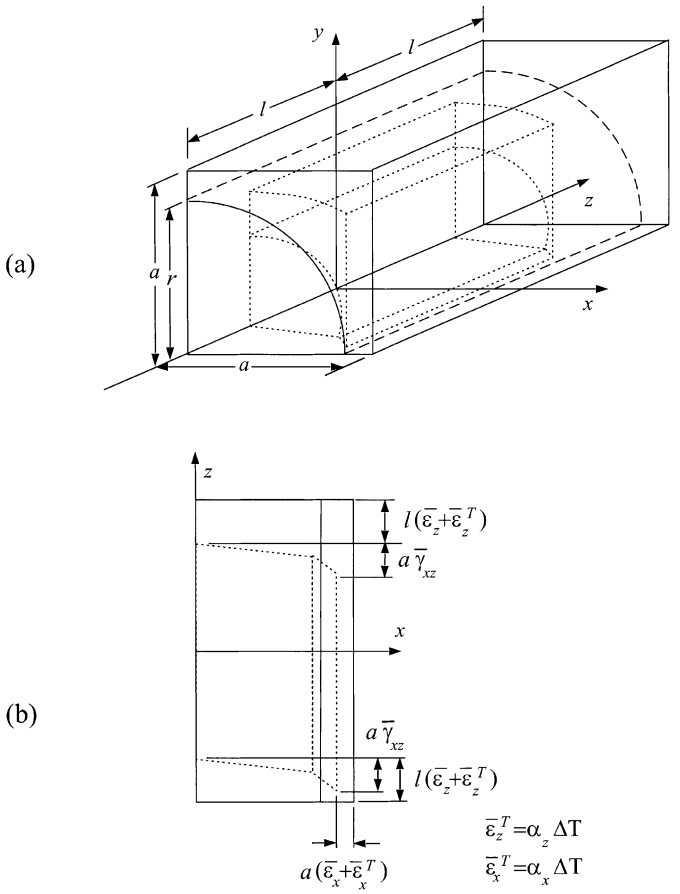

Fig. 7. Original and deformed shapes of the RVE subjected to off-axis loading: (a) complete three dimensional RVE and (b) x–z plane at $y = 0$.

where u_z is the axial displacement of a node, $\bar{\varepsilon}_z$ is the applied axial strain and $\bar{\gamma}_{zx}$ the applied axial shear strain. By combining the first two boundary conditions, appropriate constraints for the z direction are

$$\begin{aligned} u_z(x,y,l) - u_z(x,y,-l) &= 2l\bar{\varepsilon}_z, \\ u_z(a,y,z) - u_z(0,y,z) &= a\bar{\gamma}_{zx}. \end{aligned} \tag{6}$$

The first equation represents the axial load while the second equation represents axial shear loading. The axial shear constraint applied to the face (a, y, z) is compatible with the additional application of axial load.

In addition, to these constraints, all nodes with the same x and y positions on the two opposite faces of the RVE, (x, y, l) and $(x, y, -l)$, must have the same x and y displacements due to axial normal load and axial shear.

Transverse normal loading was applied to the surface (a, y, z) by applying a displacement to all nodes in the x direction. It is noted that axial and transverse loading, but not axial shear loading, cause a constant displacement in the y direction for all nodes on the face (x, a, z).

The complete boundary conditions for combined longitudinal, transverse and axial shear loading may be represented by

$$\begin{aligned} u_x(0,y,z) &= 0,\\ u_x(a,y,z) &= a\bar{\varepsilon}_x,\\ u_y(x,0,z) &= 0,\\ u_y(x,a,z) &= \text{constant},\\ u_x(x,y,-l) &= u_x(x,y,l),\\ u_y(x,y,-l) &= u_y(x,y,l),\\ u_z(x,y,-l) - u_z(x,y,l) &= 2l\bar{\varepsilon}_z,\\ u_z(a,y,z) - u_z(0,y,z) &= a\bar{\gamma}_{zx}, \end{aligned} \tag{7}$$

where a and l are geometric parameters shown in Fig. 7(a), $u_x(0,y,z)$ is the displacement component of the nodes on the plane (0, y, z) in the x direction, $\bar{\gamma}_{zx}$ is the applied axial shear strain and $\bar{\varepsilon}_x$ and $\bar{\varepsilon}_z$, the applied transverse and axial strains, respectively. By using Eq. (7), various loading conditions can be considered: pure axial shear (by applying $\bar{\varepsilon}_x = \bar{\varepsilon}_z = 0$), axial and transverse loading (by applying $\bar{\gamma}_{zx} = 0$) and any combination of these cases.

The appropriate boundary conditions for the prediction of thermal residual stress are similar to those for biaxial normal loading since, for example, the surfaces (x, y, l) and (x, y, $-l$) move towards each other due to thermal strain. Therefore, the boundary conditions may be modified easily to include thermal residual stresses:

$$\begin{aligned} u_x(0,y,z) &= 0,\\ u_x(a,y,z) &= a(\bar{\varepsilon}_x + \bar{\varepsilon}_x^{\mathrm{T}}),\\ u_y(x,0,z) &= 0,\\ u_y(x,a,z) &= \text{constant},\\ u_x(x,y,-l) &= u_x(x,y,l),\\ u_y(x,y,-l) &= u_y(x,y,l),\\ u_z(x,y,-l) - u_z(x,y,l) &= 2l(\bar{\varepsilon}_z + \bar{\varepsilon}_z^{\mathrm{T}}),\\ u_z(a,y,z) - u_z(0,y,z) &= a\bar{\gamma}_{zx}, \end{aligned} \tag{8}$$

where $\bar{\varepsilon}_x^{\mathrm{T}}$ and $\bar{\varepsilon}_z^{\mathrm{T}}$ denote the transverse and axial strains due to a temperature change with respect to the reference temperature. These thermal strains were calculated by carrying out a thermal strain analysis to evaluate the effective coefficients of thermal expansion α_x and α_z in the transverse and axial directions. Fig. 7(b) depicts the original and deformed RVE subjected to combined off-axis and thermal loading.

3.3. Interface conditions

As for the 2-D analysis for axial and transverse loading, perfectly bonded and completely de-bonded interface conditions were used for general off-axis loading. However, a perfectly de-bonded interface can only transfer compressive stress but for off-axis loading axial shear stresses can also be transferred if the interface is rough. In addition, therefore, a de-bonded interface with friction was considered for the off-axis analyses.

In this work, Coulomb friction has been used to model the load transfer at the interface, as in previous studies (Nimmer, 1990; Nimmer et al., 1991). Although there is some doubt whether a Coulomb model of friction is a wholly acceptable model at a micro-mechanical scale, the model does allow a straightforward method of varying the amount of shear stress transfer between matrix and fibre. The coefficient of friction was varied from $\mu = 0$ for a perfectly de-bonded interface to $\mu = 5$ for a high level of friction.

4. Results and discussion

4.1. Model validation

A verification of the off-axis, micro-mechanical model was first performed by checking the finite element predictions for various continuum level strain components with elasticity theory. The elastic strain components in the loading direction are (Datoo, 1991) as follows

$$\begin{aligned}
\varepsilon_1 &= \left[\frac{\cos^4\theta}{E_A} + \left(\frac{1}{G_A} - 2\frac{\nu_{AT}}{E_A}\right)\sin^2\theta\cos^2\theta + \frac{\sin^4\theta}{E_T}\right]\sigma_x^*, \\
\varepsilon_2 &= -\left[(\cos^4\theta + \sin^4\theta)\frac{\nu_{LT}}{E_A} - \left(\frac{1}{E_A} + \frac{1}{E_T} - \frac{1}{G_A}\right)\sin^2\theta\cos^2\theta\right]\sigma_x^*, \\
\gamma_{12} &= -\sin 2\theta\left[\frac{\nu_{AT}}{E_A} + \frac{1}{E_T} - \frac{1}{2G_A} - \left(\frac{1}{E_A} + \frac{1}{E_T} - \frac{1}{G_A}\right)\cos^2\theta\right]\sigma_x^*,
\end{aligned} \tag{9}$$

where E_A and E_T denote the axial ($\theta = 0°$) and transverse ($\theta = 90°$) Young's moduli and G_A and ν_{AT} are the axial shear modulus and Poisson's ratio. The strain components in the material co-ordinate system are obtained using the following transformation law:

$$\begin{aligned}
\varepsilon_x &= \varepsilon_1\cos^2\theta + \varepsilon_2\sin^2\theta + \gamma_{12}\sin 2\theta/2, \\
\varepsilon_y &= \varepsilon_1\sin^2\theta + \varepsilon_2\cos^2\theta - \gamma_{12}\sin 2\theta/2, \\
\gamma_{xy} &= (\varepsilon_2 - \varepsilon_1)\sin 2\theta + \gamma_{12}\cos 2\theta.
\end{aligned} \tag{10}$$

Values for E_A, E_T, and ν_{AT} were obtained from simple tension analyses in the axial and transverse directions, while G_A was determined using a pure axial shear analysis. The finite element model and the necessary boundary conditions for an axial shear analysis can be found elsewhere; without residual stress in Nedele and Wisnom (1994) and with residual stresses in Aghdam et al. (1998). The pure axial, transverse, and axial shear analyses with a perfectly bonded interface predicted the following elastic moduli for a SiC/Ti composite with a fibre volume fraction of 0.33:

$$\begin{aligned}
E_L &= 200.6\ \text{GPa}, \\
E_T &= 157.4\ \text{GPa}, \\
G_A &= 60.31\ \text{GPa}, \\
\nu_{LT} &= 0.265.
\end{aligned}$$

Using these values as elastic moduli of the composite in conjunction with Eqs. (9) and (10), the strain components were determined in the material co-ordinate system as a function of the fibre orientation angle, θ. Results from this macroscopic analytical model are shown in Fig. 8, compared with the predicted values obtained from the micro-mechanical finite element model. All strain components are normalised with respect to the strain in the loading direction ε_1. Results obtained from the analytical continuum model and the finite element micro-mechanical model show excellent agreement.

4.2. Stress–strain response

The stress–strain behaviour of the composite was examined for three different off-axis angles, 15°, 30° and 45°, and for different interface conditions. All results include thermal residual stress effects. Results were compared with available experimental data provided by Thomas (1997) for a SiC/Ti composite MMC

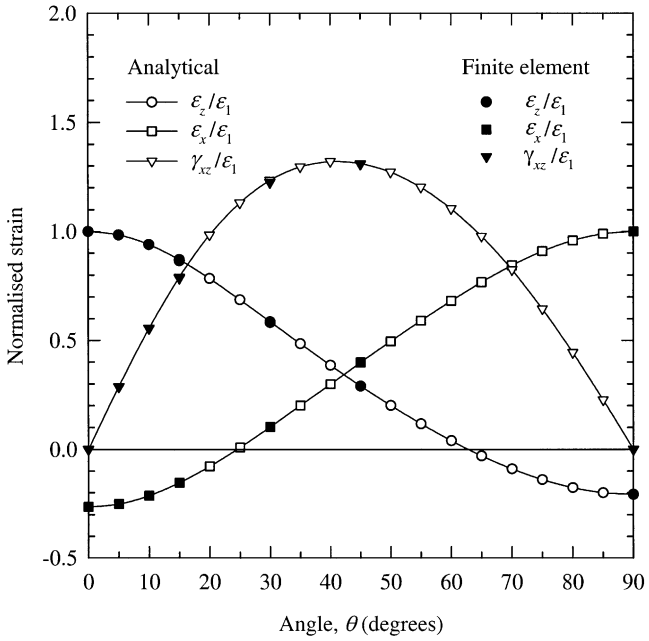

Fig. 8. Comparison of various normalised strain components for unidirectional SiC/Ti composite in off-axis tensile test.

with a fibre volume fraction of 0.33. He used rectangular specimens, 150×20 mm^2, electro-discharge machined from a plate at different angles.

Figs. 9–11 show the finite element results for off-axis angles of 15°, 30° and 45°. It is evident that neither the perfectly bonded nor the completely de-bonded analyses provide an adequate representation of the observed material behaviour. For the perfectly bonded case, the finite element results show much stiffer behaviour than experiment while for the completely de-bonded case ($\mu = 0$), the finite element results are much less stiff. The under-prediction in the completely de-bonded case must be due to transfer of shear stress between fibre and matrix, after failure of the interface. Figs. 9–11 show finite elements results for a variety of coefficients of friction, from $\mu = 0$ to $\mu = 5$. Intermediate values of friction show much better agreement with experiment, in particular a coefficient of between 1 and 2 gives acceptable results for all three off-axis angles. Again, as for transverse loading, progressive failure of the interface occurs in practice. At low loads, the experimental results lie initially on the curve for a completely bonded interface while for high loads they are close to the de-bonded curve with friction.

4.3. Young's modulus and elastic limit

When the effects of the end constraints are small, the apparent Young's modulus E_θ in an off-axis test can be determined from Eq. (9) as

$$E_\theta = \left[\frac{\cos^4\theta}{E_A} + \left(\frac{1}{G_A} - 2\frac{\nu_{AT}}{E_A} \right) \sin^2\theta \cos^2\theta + \frac{\sin^2\theta}{E_T} \right]^{-1}. \tag{11}$$

End constraint effects result in an error in E_θ when compared to experiment, but for the specimen geometry and material properties considered here the errors can be shown to be small following the calculations in Appendix A. Using the values quoted in Section 4.1 for the elastic properties of the composite, the

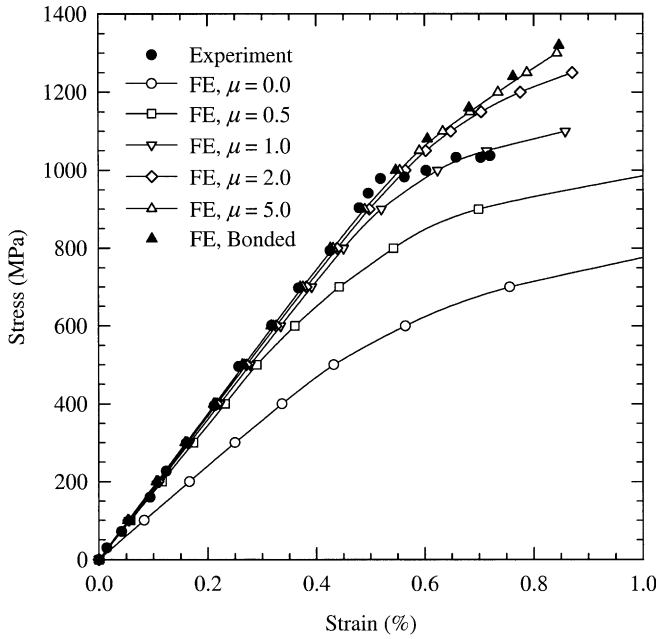

Fig. 9. Comparison between FE predictions and experimental stress–strain curves of SiC/Ti subjected to off-axis loading ($\theta = 15°$) with residual stress effects.

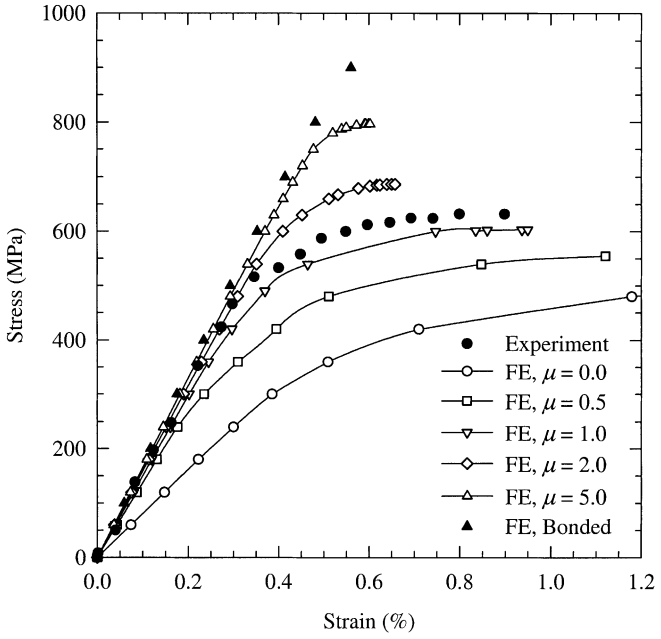

Fig. 10. Comparison between FE predictions and experimental stress–strain curves of SiC/Ti subjected to off-axis loading ($\theta = 30°$) with residual stress effects.

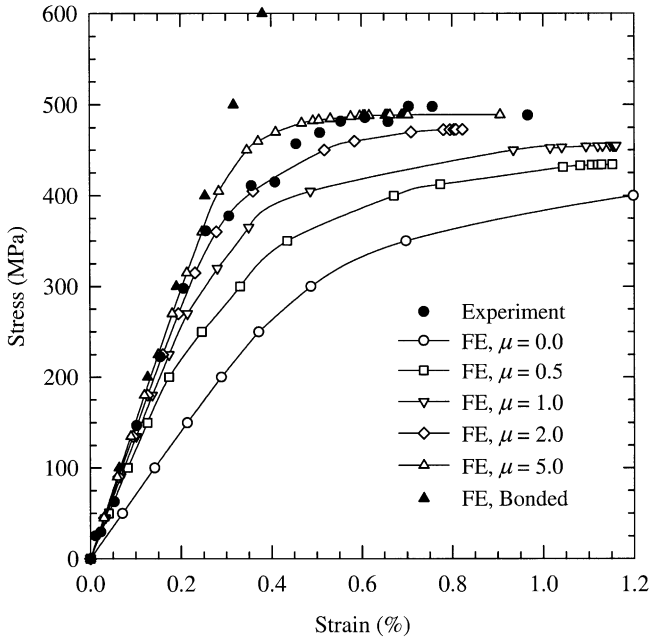

Fig. 11. Comparison between finite element predictions and experimental stress–strain curves of SiC/Ti subjected to off-axis loading ($\theta = 45°$) with residual stress effects.

analytical predictions for off-axis Young's modulus of SiC/Ti MMC with a fibre volume fraction of 0.33 were determined. Fig. 12 compares these analytical predictions with experimental data (Thomas and Winstone, 1998) and finite element results for off-axis angles between 0° and 90°. The finite element results for a bonded interface are in good agreement with the analytical predictions, but the results for a de-bonded interface with friction given by $\mu = 1.0$ are closer to experimental data.

Fig. 13 is a graph of the elastic limit versus off-axis angle from 0° to 90° obtained from the finite element model and experimental results. The elastic limit, that is the stress for the onset of non-linear behaviour, was obtained from the stress–strain curves using a 0.2% proof strain. The perfectly bonded interface gives a good agreement for small off-axis angles up to about 10–15°, since the non-linear behaviour is caused principally by matrix plasticity. At higher off-axis angles, interface failure is an important cause of non-linearity and the de-bonded predictions are closer to experimental results, particularly for a frictional interface.

Of interest in Fig. 13 is the increase in the elastic limit as θ increases from 0° up to about 10°. A possible reason for this behaviour is the presence of thermal residual stresses within the matrix. Indeed, a finite element prediction of the elastic limit was carried without thermal residual stresses and showed no such increase.

4.4. Tensile strength

Predictions about the strength of SiC/Ti based on finite element analysis are compared to the experimental data (Thomas, 1997) in Fig. 14 for a perfectly bonded interface and a de-bonded interface with friction. Depending on the loading angle, strength was controlled either by fracture of the fibres or by yield of the matrix. The finite element results were calculated from the load at which the fibre fracture stress was

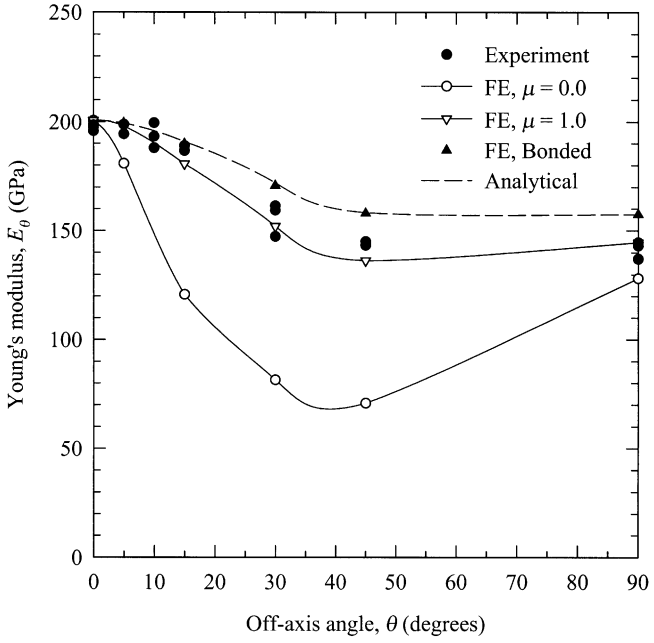

Fig. 12. Comparison of off-axis Young's modulus for SiC/Ti MMC.

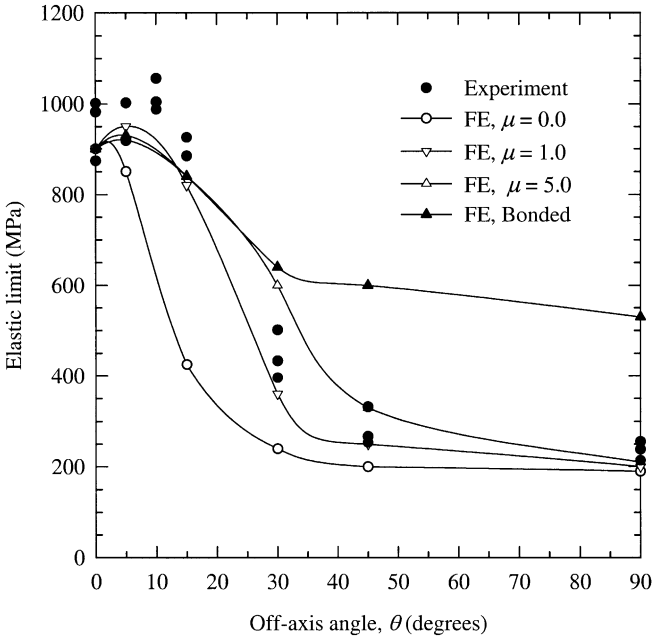

Fig. 13. Comparison of onset of non-linearity in SiC/Ti MMC subjected to off-axis loading.

exceeded, or from the load at which the stress–strain curve became horizontal. The fracture stress of the DERA Sigma SM1240 fibres, C/TiB$_x$ coated SiC, was taken to be 3240 MPa, (Robertson, 1995).

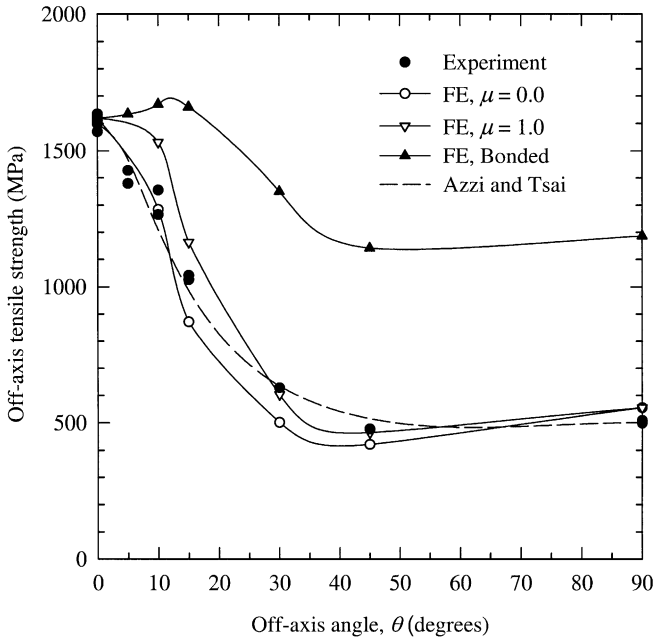

Fig. 14. Comparison of tensile strength for SiC/Ti MMCs subjected to off-axis loading with thermal residual stress effects.

Thermal stresses were included in the finite element analysis since, although they do not affect the strength for the perfectly bonded case, they are important when imperfect bonding occurs. Residual stresses at the interface are highly compressive which tends to delay separation of the fibre and matrix (Nimmer, 1990; Li and Wisnom, 1995) and allow more transfer of shear stress.

Several failure criteria have been proposed to predict the off-axis strength of fibre reinforced composites. Azzi and Tsai (1965) adopted Hill's (1950) failure criterion to develop a model that predicts the strength of laminates and unidirectional composite subjected to a general state of stress. Their general model can be reduced to a simple equation for prediction of the strength of a unidirectional composite in an off-axis tension test:

$$\sigma_\theta = \left[\frac{\cos^4\theta}{\sigma_{c0}^2} + \left(\frac{1}{\tau_c^2} - \frac{1}{\sigma_{c0}^2} \right) \sin^2\theta \cos^2\theta + \frac{\sin^4\theta}{\sigma_{c90}^2} \right]^{-1/2}, \tag{12}$$

where σ_θ represents the off-axis strength and σ_{c0}, σ_{c90} and τ_c the axial, transverse, and shear strengths. Values for the axial and transverse strengths in Eq. (12) were taken from the experimental results of 1620 and 498 MPa, respectively. A value for the shear strength was taken to be 287 MPa from Thomas and Winstone (1998). The predicted strength curve obtained from Eq. (12) is compared in Fig. 14 with the experimental results with good agreement.

5. Conclusions

2-D micro-mechanical models of fibre reinforced composites have been developed using the finite element method. The models allowed the analysis of composite materials subjected to axial and transverse

loading. The effects of de-bonding of the interface and thermal residual stress were included. The results of the micro-mechanical models showed excellent agreement with experimental results of SiC/Ti MMCs.

Micro-mechanical models have also been developed using a 3-D finite element approach. These 3-D models allow the behaviour of the composite to be predicted under combinations of axial and transverse loading and axial shear. Again, the effects of interface de-bonding and thermal residual stress have been included. In particular, the 3-D models allows the prediction of the behaviour of composite in off-axis loading.

The predictions of the 3-D micro-mechanical model have been compared with experimental results for the off-axis behaviour of MMCs. Excellent agreement was found for the stress–strain behaviour, Young's modulus, elastic limit and tensile strength. It was found that predictions for a perfectly bonded interface were valid for lower loads whereas predictions for a de-bonded interface were better for high loads. Friction between fibre and matrix and the presence of thermal residual stress had to be included in the case of a de-bonded interface to achieve good results.

Acknowledgements

The first author wishes to acknowledge a Ph.D. scholarship provided by Amir-kabir University of Technology in Tehran. Additional financial support was provided by the University of Bristol. We are also grateful to Dr M.P. Thomas at DERA, Farnborough, UK for allowing us to use his experimental results.

Appendix A. End constraint effects in off-axis loading of unidirectional MMC's

In off-axis tensile loading of a composite, the shear coupling term tends to distort the flat rectangular specimen to a parallelogram. Additional forces and bending moments are required at the ends of the specimen when rotation is constrained (Pagano and Halpin, 1968). The stress components at the midpoint of the specimen in the loading co-ordinate system when rotation is constrained are as follows:

$$\begin{aligned}\sigma_1 &= \sigma_1^*(1-2\eta/3)^{-1},\\ \sigma_2 &= 0,\\ \tau_{12} &= -\frac{\overline{S}_{11}}{\overline{S}_{16}}\eta\sigma_1 = -\frac{\overline{S}_{11}\eta}{\overline{S}_{16}(1-2\eta/3)}\sigma_1^*,\end{aligned} \tag{A.1}$$

where σ_1^* denotes the average stress, determined by dividing the applied load to the cross-section of the specimen, $\overline{S}_{ij}$ are the compliance coefficients with respect to the loading co-ordinate system which can be determined from principal compliance matrix in the material co-ordinate system, and η is the error caused when end constraints effects are ignored, i.e.

$$\eta = \frac{6\overline{S}_{16}^2}{\overline{S}_{11}(6\overline{S}_{66}+\overline{S}_{11}l^2/h^2)}, \tag{A.2}$$

where symbols l and h are the length and half-width of the specimen.

Using the transformation law, the stress components at midpoint of the specimen in the material principal co-ordinate system are

$$\sigma_x = \frac{\sigma_1^*}{1-2\eta/3}\left[\sin^2\theta + \frac{\overline{S}_{11}\eta}{\overline{S}_{16}}\sin 2\theta\right],$$
$$\sigma_z = \frac{\sigma_1^*}{1-2\eta/3}\left[\cos^2\theta - \frac{\overline{S}_{11}\eta}{\overline{S}_{16}}\sin 2\theta\right], \tag{A.3}$$
$$\tau_{zx} = -\frac{\sigma_1^*}{1-2\eta/3}\left[\frac{\sin 2\theta}{2} + \frac{\overline{S}_{11}\eta}{\overline{S}_{16}}\cos 2\theta\right].$$

Correction factors for all three stress components to be evaluated are

$$\frac{\sigma_x}{\sigma_x^*} = \frac{1}{1-2\eta/3}\left[1 + 2\frac{\overline{S}_{11}\eta}{\overline{S}_{16}}\cot\theta\right],$$
$$\frac{\sigma_z}{\sigma_z^*} = \frac{1}{1-2\eta/3}\left[1 - 2\frac{\overline{S}_{11}\eta}{\overline{S}_{16}}\tan\theta\right], \tag{A.4}$$
$$\frac{\tau_{zx}}{\sigma_{zx}^*} = \frac{1}{1-2\eta/3}\left[1 + 2\frac{\overline{S}_{11}\eta}{\overline{S}_{16}}\cot 2\theta\right],$$

where, for example, σ_x is the transverse stress corrected for the end constraint effect and σ_x^*, the stress calculated from Eq. (1). The term relating to axial shear has been derived previously by Pindera and Herakovich (1986).

The correction factors defined in Eqs. (A.4) were evaluated for the aspect ratio $l/h = 15$ in the experimental results used for comparison (Thomas, 1997; Thomas and Winstone, 1998). The maximum error was found to be less than 3.6% for the complete range of fibre angles. Therefore, the results presented in this study were not corrected for the effect of end constraint.

References

ABAQUS User Manual 1997. Hibbitt, Karlsson, Sorensen, Inc., 1080 Main Street, Pawtucket, RI.

Aboudi, J., 1988. Micro-mechanical analysis of the strength of unidirectional fibre composites. Composite Science and Technology 33, 79–96.

Aboudi, J., 1989. Micro-mechanical analysis of composites by the method of cells. Applied Mechanics Review 42, 193–221.

Adams, D.F., Crane, D.A., 1984a. Combined loading micro-mechanical analysis of a unidirectional composite. Composites 15, 181–191.

Adams, D.F., Crane, D.A., 1984b. Finite element micro-mechanical analysis of a unidirectional composite including longitudinal shear loading. Computers and Structures 18, 1153–1165.

Adams, D.F., Doner, D.R., 1967. Longitudinal shear loading of a unidirectional composite. Journal of Composite Materials 1, 4–17.

Aghdam, M.M., Pavier, M.J., Smith, D.J., 1998. Micro-mechanical modelling of metal matrix composites subjected to combined thermal and shear loading. Proceedings of the sixth international conference on computer methods in composite materials, CADCOMP 98, Montreal, Canada, pp. 321–330.

Aghdam, M.M., Smith, D.J., Pavier, M.J., 2000. Finite element micro-mechanical modelling of yield and collapse behaviour of metal matrix composites. Journal of the Mechanics and Physics of Solids 43, 499–528.

Azzi, V.D., Tsai, S.W., 1965. Anisotropic strength of composites. Experimental Mechanics 5, 283–288.

Calvo, E.A., Salazar, J.M., Urena, A., Carrion, J.G., 1992. Diffusion bonding of Ti-6Al-4V alloy at low temperature metallurgical aspects. Journal of Materials Science 27, 391–398.

Chamis, C.C., Sinclair, J.H., 1976. 10 off-axis tensile test for interlaminar shear characterization of fibre composites. NASA Tech. Note D-8215.

Chamis, C.C., Sinclair, J.H., 1977. Ten-deg off-axis test for shear properties in fibre composites. Experimental Mechanics 17, 339–346.

Chandra, N., Ananth, C.R., Garmestani, H., 1994. Micro-mechanical modelling of process-induced residual stresses in SCS-6/Ti-24AL-11Nb composite. Journal of Composites Technology and Research 16, 37–46.

Clyne, T.W., Withers, P.J., 1993. An Introduction to Metal Matrix Composites. Cambridge University Press, Cambridge, UK.

Cooper, G.A., 1966. Orientation effects in fibre-reinforced metals. Journal of the Mechanics and Physics of Solids 14, 103–111.

Datoo, M.H., 1991. Mechanics of Fibrous Composites, Elsevier Science Pub. Ltd., London, UK.

Du, Z.Z., Zok, F.W., 1998. Limit stress conditions for weakly bonded fibre composites subjected to transverse biaxial tensile loading. International Journal of Solids and Structures 35, 2821–2842.

Foye, R.L., 1973. Theoretical post-yielding behaviour of composite laminates part I – Inelastic micro-mechanicas. Journal of Composite Materials 7, 179–193.

Hill, R., 1950. The Mechanical Theory of Plasticity. Oxford Univ. Press, London.

IMI Titanium Ltd. Brochure, 1993. High temperature alloys.

Jackson, P.W., Cratchley, D., 1966. The effects of fibre orientation on the tensile strength of fibre-reinforced metals. Journal of the Mechanics and Physics of Solids 14, 49–64.

Jansson, S., Deve, H.E., Evans, A.G., 1991. The anisotropic mechanical properties of a Ti matrix composite reinforced with SiC fibres. Metallurgical Transactions A 22A, 2975–2984.

Johnson, W.S., Lubowinski, S.J., Highsmith, A.L., 1990. Mechanical characterisation of unnotched SCS6/Ti-15-3 metal matrix composites at room temperature. In: Kennedy, J.M., Moeller, H.H., Johnson, W.S. (Eds.), Thermal and Mechanical Behaviour of Metal Matrix and Ceramic Matrix Composites, ASTM STP 1080, American Society for Testing and Materials, Philadelphia, pp. 193–218.

Kelly, A., Davis, G.J., 1965. The principles of the fibre reinforcement of metals. Metalurgical Reviews 10, 1–77.

Lekhnitskii, S.G., 1963. In: Brandstatter, J.J. (Ed.), Theory of Elasticity of an Anisotropic Elastic Body, Holden-Day, San Francisco. (Fern, P., Trans.).

Le Petitcorps, Y., Lahaye, M., Pailler, R., Naslain, R., 1988. Modern boron and SiC CVD filaments: A comparative study. Composite Science and Technology 32, 31–55.

Li, D.S., Wisnom, M.R., 1995. Factors controlling the transverse tensile properties of unidirectional SiC/Ti 6Al-4V. Composite Engineering 5, 235–255.

Naik, R.A., Crews, J.H., 1993. Micro-mechanical analysis of fibre–matrix interface stresses under thermomechanical loading. E.T. Camponeschi, Jr. (Ed.), Composite Materials: Testing and Design, vol. 11, ASTM STP 1206, American Society for Testing and Materials, Philadelphia, 205–219.

Nedele, M.R., Wisnom, M.R., 1994. Finite element micro-mechanical modelling of a unidirectional composite subjected to shear loading. Composites 25, 263–272.

Newaz, G.M., Zhang, K.E., 1998. Inelastic response of off-axis MMC lamina. Journal of Engineering Materials and Technology 120, 163–169.

Nimmer, R.P., 1990. Fibre–matrix interface effects in the presence of thermally induced residual stress. Journal of Composite Technology and Research 12, 65–75.

Nimmer, R.P., Bankert, R.J., Russell, E.S., Smith, G.A., Wright, P.K., 1991. Micro-mechanical modelling of fibre/matrix interface effects in transversely loaded SiC/Ti-6-4 metal matrix composites. Journal of Composite Technology and Research 13, 3–13.

Pagano, N.J., Halpin, J.C., 1968. Influence of end constraint in the testing of anisotropic bodies. Journal of Composite Materials 2, 18–31.

Pindera, M.J., 1989. Shear testing of fibre reinforced metal matrix composites. In: Johnson, W.S. (Ed.), Metal Matrix Composites: Testing, Analysis, and Failure Modes, ASTM STP 1032, American Society for Testing and Materials, Philadelphia, pp. 19–42.

Pindera, M.J., Herakovich, C.T., 1986. Shear characterisation of unidirectional composites with the off-axis test. Experimental Mechanics 26, 103–112.

Pindera, M.J., Choksi, G., Hidde, J.S., Herakovich, C.T., 1987. A methodology for accurate shear characterisation of unidirectional composites. Journal of Composite Materials 21, 1164–1184.

Pipes, R.B., Cole, B.W., 1973. On the off-axis strength test for anisotropic materials. Journal of Composite Materials 7, 246–256.

Rizzo, R.R., 1969. More on the influence of end constraints on off-axis tensile tests. Journal of Composite Materials 3, 202–219.

Robertson, J., 1995. Private communication, DERA Sigma Fibre Composites, DERA, Farnbourough, UK.

Spowart, J.E., Clyne, T.W., 1999. The axial compressive failure of titanium reinforced with silicon carbide monofilaments. Acta Materialia 47, 671–687.

Stowell, E.Z., Liu, T.S., 1961. On the mechanical behaviour of fibre-reinforced crystalline materials. Journal of the Mechanics and Physics of Solids 9, 242–260.

Sun, C.T., Vaidya, R.S., 1996. Prediction of composite properties from a representative volume element. Composite Science and Technology 56, 171–179.

Thomas, M.P., 1997. Tensile properties of Ti-6-4/ SM1240 titanium metal matrix composite with off-axis fibres. SMC Technical report No. DERA/SMC/SM2/TR 970145, Defence Evaluation and Research Agency, Farnborough, UK.

Thomas, M.P., Winstone, M.R., 1998. Effect of the angle between fibres and tensile axis on static properties of unidirectional reinforced titanium MMC. Proceedings of the European Conference on Composite Materials (ECCM-8), Naples, Italy, 4, 147–154.

Wisnom, M.R., 1990. Factors affecting the transverse tensile strength of unidirectional continuous silicon carbide fibre reinforced 6061 Aluminium. Journal of Composite Materials 24, 707–726.

Zahl, D.B., Schmauder, S., McMeeking, M.R., 1994. Transverse strength of metal matrix composites reinforced with strongly bonded continuous fibres in regular arrangements. Acta Metallurgica et Materialia 42, 2983–2997.